



Original article

Design and synthesis of hybrid solids based on the tetravanadate core toward improved catalytic properties



Yan-Hong Niu, Song Yang, Ji-Kun Li, Yan-Qing Xu*, Chang-Wen Hu*

Key Laboratory of Cluster Science, Ministry of Education of China, Beijing Key Laboratory of Photoelectronic/Electrophotonic, School of Chemistry, Beijing Institute of Technology, Beijing 100081, China

ARTICLE INFO

Article history:

Received 26 October 2015

Received in revised form 14 December 2015

Accepted 30 December 2015

Available online 13 January 2016

Keywords:

Hybrid

Tetravanadate core

Heterogeneous catalysis

Olefin epoxidation

ABSTRACT

Five inorganic–organic hybrid vanadates based on tetravanadate cores, transition metals and N-donor ligands have been designed and synthesized under hydrothermal conditions, namely, $[\text{Zn}(\text{eIM})_3]_2\text{V}_4\text{O}_{12}$ (**1**), $[\text{Zn}(\text{pIM})_3]_2\text{V}_4\text{O}_{12} \cdot \text{H}_2\text{O}$ (**2**), $[\text{Zn}(\text{ipIM})_3]_2\text{V}_4\text{O}_{12}$ (**3**), $[\text{Co}(\text{eIM})_3]_2\text{V}_4\text{O}_{12} \cdot \text{H}_2\text{O}$ (**4**), $[\text{Cu}(\text{eIM})_2(\text{H}_2\text{O})]_2\text{V}_4\text{O}_{12}$ (**5**) (eIM = 1-ethylimidazole, pIM = 1-propylimidazole, ipIM = isopropylimidazole). All compounds were fully characterized by single-crystal XRD, powder XRD, elemental analysis, TGA, and FT-IR spectroscopy. The hybrid zinc vanadates (**1–3**) and cobalt vanadate (**4**) exhibit interesting 2D folded structures and the hybrid copper vanadate (**5**) presents a 1D chain configuration. All compounds can catalyze olefin epoxidation reactions when using TBHP (TBHP = *tert*-butyl hydroperoxide) as an oxidant in acetonitrile. The introduction of transition metal ions into tetravanadate cores not only improved the catalytic activity but also fulfilled the heterogeneous catalytic behavior. **1–5** all exhibit extraordinary efficiency in converting olefins to the corresponding epoxides with high conversion and selectivity (particularly, conv. up to 97.1%, sele. up to 100% for **1**). Leaching test was also carried out to prove the heterogeneous behavior.

© 2016 Chinese Chemical Society and Institute of Materia Medica, Chinese Academy of Medical Sciences.

Published by Elsevier B.V. All rights reserved.

1. Introduction

Oxidation reactions, such as the oxidation of C–H bonds, hydroxylation, epoxidation, and oxidation of heteroatom-based substrates, are very valuable processes in biology, chemistry, and industry [1–4]. Among them, the epoxidation of alkenes attracts continuing interest owing to the importance of epoxides as key chemical intermediates for a wide variety of industrial and chemical applications [5–8]. Up to now a large number of efficient methods for the epoxidation of alkenes with transition-metal catalysts, such as Ti, V, Mn, Te, W, Re, Pt, have been developed [9]. However, most of them are homogeneous and require tedious separation of the expensive catalyst [10]. Therefore, developing highly active, widely applicable heterogeneous and easily recycled catalysts for epoxidation is still desirable.

As a new generation of solid-state materials, polyoxovanadates (POVs) have been developed not only for their various fascinating framework topologies, but also for their potential application in the fields of magnetism, electrical conductivity,

catalysis and photochemistry [11–13]. Recently our group has reported three new organic functionalized POVs with imidazole ligands, $\text{V}^{\text{V}}_6\text{O}_{15}(\text{mIM})_8$, $\text{V}^{\text{IV}}_2\text{V}^{\text{V}}_4\text{O}_{14}(\text{mIM})_8$, $\text{V}^{\text{IV}}_2\text{V}^{\text{V}}_4\text{O}_{14}(\text{mIM})_8$ (mIM: 1-methylimidazole, eIM: 1-ethylimidazole), which are highly efficient and selective catalysts for the oxidation of benzyl alcohols [14]. To further promote the catalytic activity of POV complexes and guarantee the heterogeneity during the catalytic process, transition-metal species have been introduced into the POVs system and led to a variety of novel heterogeneous catalysts [15–20]. For example, Arriortua et al. reported three isostructural vanadate compounds of $\text{M}(\text{HAep})_2(\text{VO}_3)_4$ (M=Co, Ni, Cu; Aep = 1-(2-aminoethyl) piperazine) compounds, which display efficient catalytic activity for alkyl and aryl sulfides [15]. Recently, our group prepared three inorganic–organic hybrid vanadates $[\text{Co}_2(\text{mIM})_5(\text{H}_2\text{O})_2]\text{V}_4\text{O}_{12}$, $[\text{Ni}_2(\text{mIM})_7(\text{H}_2\text{O})]\text{V}_4\text{O}_{12} \cdot \text{H}_2\text{O}$ and $[\text{Cd}(\text{eIM})_2(\text{H}_2\text{O})]\text{V}_2\text{O}_6$ with chiral 3D framework, 2D folded network and 1D ladder chain architectures using a hydrothermal synthetic approach under different conditions [21], and another study of Cu-vanadate showed much better catalytic activity for the selective oxidation of sulfides and alcohols than the vanadate alone [22]. Such strategy is also adopted in the catalytic epoxidation reactions [23–26]. Palaniandavar reported a family of Mn(III) complexes $[\text{Mn}(\text{L})\text{Cl}]$ of

* Corresponding authors.

E-mail addresses: xyq@bit.edu.cn (Y.-Q. Xu), cw.hu@bit.edu.cn (C.-W. Hu).

linear bis(phenolate) ligands, which displays selective catalytic activity for the epoxidation of olefins [26]. Inspired by these work, we tried to introduce transition metal ions into the title tetravanadate cores to obtain hybrid vanadates, which might be a feasible way to improve the catalytic property in the epoxidation of olefins.

Herein, using similar hydrothermal synthetic approach, we successfully grafted different transition metal ions into POVs to synthesize a series of organic-inorganic hybrid vanadates $[\text{Zn}(\text{eIM})_3]_2\text{V}_4\text{O}_{12}$ (**1**), $[\text{Zn}(\text{pIM})_3]_2\text{V}_4\text{O}_{12} \cdot \text{H}_2\text{O}$ (**2**), $[\text{Zn}(\text{ipIM})_3]_2\text{V}_4\text{O}_{12}$ (**3**), $[\text{Co}(\text{eIM})_3]_2\text{V}_4\text{O}_{12} \cdot \text{H}_2\text{O}$ (**4**), $[\text{Cu}(\text{eIM})_2(\text{H}_2\text{O})]_2\text{V}_4\text{O}_{12}$ (**5**), (eIM = 1-ethylimidazole, pIM = 1-propylimidazole, ipIM = isopropylimidazole). By introducing Co^{2+} , Cu^{2+} and Zn^{2+} as structural connection nodes, the polyhedral fragments of tetravanadate $[\text{V}_4\text{O}_{12}]^{4-}$ units were linked together to create 2D network architectures and 1D chain structures, respectively. All compounds were fully characterized by single-crystal X-ray diffraction (SXRD), powder X-ray diffraction (PXRD), elemental analyses, TGA and FT-IR spectroscopy. Further, not only the catalytic activity of these compounds in the olefin epoxidation proved to be improved greatly, but also the catalysts can be reused without losing their activity after three cycles and can function as heterogeneous catalysts, which may have potential applications in the industry. To our knowledge, this is the first time that inorganic–organic hybrid vanadates were used as catalysts in the olefin epoxidation.

2. Experimental

2.1. Materials and general methods

All chemicals and reagents were commercially obtained and used without further purification. All syntheses were carried out in 20 mL Teflon-lined stainless steel containers under autogenous pressure. The mixed reactants were stirred at room temperature for 120 min before heating. The FT-IR spectra were recorded using KBr pellets in the range of $4000\text{--}400\text{ cm}^{-1}$ on a Nicolet 170 SXFT/IR spectrometer. The X-ray powder diffraction (XPRD) of samples was collected on a Bruker D8 X-ray diffractometer equipped with a graphite monochromatized $\text{Cu K}\alpha$ radiator ($\lambda = 0.15418\text{ \AA}$). The TGA was performed on a DTG-60 AH instrument under a N_2 atmosphere with a heating rate of $10\text{ }^\circ\text{C/min}$. Elemental (C, H and N) analyses were performed on a PerkinElmer 2400 II analyzer. The metal contents of the compounds **1–5** were measured by inductively coupled plasma (ICP) on a JY-ULTIMA2 analyzer. After the catalytic reaction was completed, the resulting mixture was analyzed by GC–MS and GC using naphthalene as an internal standard substrate. The GC analyses were performed on a Shimadzu GC-2014C with an FID detector equipped with an Rtx-1701 Sil capillary column. The GC–MS spectra were recorded on an Agilent 7890A-5975C at an ionization voltage of 1200 V. Atomic absorption analysis were measured by an inductively coupled plasma spectrometer (ICP) on an ICP-6000 analyzer.

2.2. Synthesis of $[\text{Zn}(\text{eIM})_3]_2\text{V}_4\text{O}_{12}$ (**1**)

A mixture of $\text{Zn}(\text{CH}_3\text{COO})_2 \cdot 2\text{H}_2\text{O}$ (0.1705 g, 0.8 mmol), NH_4VO_3 (0.1404 g, 0.8 mmol), eIM (0.3 mL), and H_2O (8 mL) was heated at about $120\text{ }^\circ\text{C}$ for 72 h. After the mixture was cooled to room temperature, yellow crystals were isolated from the mixture. Yield: 76% (based on NH_4VO_3); Anal. Calcd. for $\text{C}_{30}\text{H}_{48}\text{Zn}_2\text{N}_{12}\text{V}_4\text{O}_{12}$ (%): C, 32.63; H, 4.35; N, 15.23. Found: C, 32.76; H, 4.41; N, 15.21.

2.3. Synthesis of $[\text{Zn}(\text{pIM})_3]_2\text{V}_4\text{O}_{12} \cdot \text{H}_2\text{O}$ (**2**)

Compound **2** was synthesized by almost the same procedure as compound **1** except eIM was replaced by ipIM, and the amount was

reduced to 0.2 mL. After the mixture was cooled to room temperature, yellow crystals were isolated from the mixture. Yield: 68% (based on NH_4VO_3); Anal. Calcd. for $\text{C}_{36}\text{H}_{64}\text{Zn}_2\text{N}_{12}\text{O}_{14}\text{V}_4$ (%): C, 35.3; H, 5.23; N, 13.73. Found: C, 35.36; H, 5.26; N, 13.61.

2.4. Synthesis of $[\text{Zn}(\text{ipIM})_3]_2\text{V}_4\text{O}_{12}$ (**3**)

Compound **3** was synthesized by almost the same procedure as compound **1** except the amount of eIM was reduced from 0.3 mL to 0.2 mL. After the mixture was cooled to room temperature, yellow crystals were isolated from the mixture. Yield: 70% (based on NH_4VO_3); Anal. Calcd. for $\text{C}_{36}\text{H}_{60}\text{Zn}_2\text{N}_{12}\text{O}_{12}\text{V}_4$ (%): C, 36.38; H, 5.05; N, 14.14. Found: C, 36.52; H, 5.07; N, 14.19.

2.5. Synthesis of $[\text{Co}(\text{eIM})_3]_2\text{V}_4\text{O}_{12} \cdot \text{H}_2\text{O}$ (**4**)

A mixture of $\text{CoCl}_2 \cdot 6\text{H}_2\text{O}$ (0.1705 g, 0.8 mmol), NH_4VO_3 (0.1404 g, 0.8 mmol), eIM (0.8 mL), and H_2O (8 mL) was heated at about $120\text{ }^\circ\text{C}$ for 72 h. After the mixture was cooled to room temperature, dark purple crystals were isolated from the mixture. Yield: 62% (based on NH_4VO_3); Anal. Calcd. for $\text{C}_{30}\text{H}_{52}\text{Co}_2\text{N}_{12}\text{O}_{14}\text{V}_4$ (%): C, 31.96; H, 4.61; N, 14.91. Found: C, 31.71; H, 4.42; N, 14.58.

2.6. Synthesis of $[\text{Cu}(\text{eIM})_2(\text{H}_2\text{O})]_2\text{V}_4\text{O}_{12}$ (**5**)

A mixture of $\text{CuCl}_2 \cdot 2\text{H}_2\text{O}$ (0.1705 g, 0.8 mmol), NH_4VO_3 (0.1404 g, 0.8 mmol), eIM (0.7 mL), and H_2O (8 mL) was heated at about $120\text{ }^\circ\text{C}$ for 72 h. After the mixture was cooled to room temperature, green crystals were isolated from the mixture. Yield: 68% (based on NH_4VO_3); Anal. Calcd. for $\text{C}_{20}\text{H}_{36}\text{Cu}_2\text{N}_8\text{O}_{14}\text{V}_4$ (%): C, 25.44; H, 3.82; N, 11.87. Found: C, 25.65; H, 3.74; N, 11.75.

2.7. Catalyzed epoxidation of olefin

Compound **1** (0.01 mmol, 5.0 mg), olefin (1 mmol), TBHP (*tert*-butyl hydroperoxide, 2 mmol), acetonitrile (2 mL) were added to a glass tube, then the catalytic reaction was performed on a Wattecs Parallel Reactor at $75\text{ }^\circ\text{C}$ for 24 h. After the reaction was completed, the resulting mixture was analyzed by GC–MS and GC.

2.8. X-ray crystallography

The single-crystal XRD data of all compounds were collected on a Bruker APEX-II CCD detector with graphite monochromatic $\text{Mo K}\alpha$ radiation ($\lambda = 0.71073\text{ \AA}$) at room temperature. Crystals were mounted on a glass fiber and coated with oil. All absorption corrections were performed using a multiscan technique. The reflections collected were integrated and scaled using the APEX 2 software package [27,28]. All crystal structures were solved by the direct method and refined by full-matrix least-squares on F^2 using the SHELXTL program package (Bruker) [27,28]. All of the non-hydrogen atoms were located by the direct methods and were refined anisotropically. All hydrogen atoms were fixed at calculated position and refined as riding models. The crystallographic data have been deposited with the Cambridge Crystallographic Data Centre (CCDC), CCDC-1058623 (**1**), CCDC-1058590 (**2**), CCDC-1058657 (**3**), CCDC-1404876 (**4**), CCDC-1404877 (**5**). The crystallographic details of **1–5** are summarized in Table S1 (Supporting information).

3. Results and discussion

3.1. Synthesis

At present, many inorganic–organic hybrid vanadates with a variety of structures have been synthesized using the hydrother-

mal methods. In most cases, controlling the synthesis of the hybrid vanadates is very difficult, because the architecture of the final product depends on many factors, such as the type of transition metals, starting materials, ligands, ratio of reactants and the reacting temperature, etc. [21]. Yet, it is possible to partially control the synthesis of these compounds by adjusting the initial reaction conditions. Herein, we chose the vanadium source NH_4VO_3 as the precursors in the synthetic process to react with $\text{Zn}(\text{CH}_3\text{COO})_2 \cdot 2\text{H}_2\text{O}$, $\text{CoCl}_2 \cdot 6\text{H}_2\text{O}$, $\text{CuCl}_2 \cdot 2\text{H}_2\text{O}$ in the presence of the N-donor ligands eIM, pIM or ipIM under hydrothermal conditions. Fortunately, we successfully prepared hybrid zinc vanadates (**1–3**), cobalt vanadate (**4**) compounds with 2D network and copper vanadate (**5**) compound with 1D chain supramolecular structure containing $[\text{V}_4\text{O}_{12}]^{4-}$ unit by changing the type of transition metals and N-donor ligands. Besides, parallel experiments of some other metal salts like $\text{Cd}(\text{CH}_3\text{COO})_2 \cdot 2\text{H}_2\text{O}$, MnCl_2 , $\text{Ni}(\text{CH}_3\text{COO})_2 \cdot 4\text{H}_2\text{O}$ etc. were also carried out in this reaction system, but unfortunately, the corresponding crystal structures were not obtained.

For zinc vanadates (**1–3**), we synthesized the comparable structures only by changing the type of ligands. As the reaction conditions are the same in the experiments, when we choose the transition Co^{2+} instead of Zn^{2+} , 2D compound **4** with a similar structure to that of compound **3** was obtained. In addition, compound **5** with a 1D chain structure can be prepared by reducing the dosage of eIM and changing the transition metal ion with the rest of the synthetic conditions remaining unchanged. Therefore, the type of metal ions and the volume of eIM are important factors in the synthesis of these compounds.

3.2. Structure description of compounds **1–4**

Single-crystal X-ray diffraction analysis reveals that the compounds **1** and **4** are isostructural with only slight differences in central metal, whose general formula can be described as $[\text{M}(\text{eIM})_3]_2\text{V}_4\text{O}_{12}$ ($\text{M}=\text{Zn}$ for **1**, Co for **4**). Compounds **1**, **2** and **3** are isostructural with differences only in ligands, which can be described as $[\text{Zn}(\text{X})_3]_2\text{V}_4\text{O}_{12}$ ($\text{X}=\text{eIM}$ for **1**, pIM for **2**, ipIM for **3**). So we will discuss the structure of **1** as an example in detail. The SXRD analysis reveals that compound **1** with an interesting 2D folded structure and crystallizes in the Orthorhombic space group Pbca . As shown in Fig. 1, the asymmetric unit of **1** consists of Zn^{2+} cations, eIM ligands and $[\text{VO}_4]$ tetrahedra. In Fig. 1, there are four five-coordinated crystallographically independent $\text{Zn}(\text{II})$ ions in compound **1**, the $\text{Zn}(\text{II})$ ion defined by three nitrogen atoms from eIM ligands and two oxygen atoms from two tetrahedral $[\text{VO}_4]$ ions. In the secondary building $[\text{V}_4\text{O}_{12}]^{4-}$ cluster, there are four $[\text{VO}_4]$ tetrahedrons through the corner-sharing bridge O atoms and coordinates with a Zn^{2+} ion via one of the terminal O atoms. It is worth mentioning that in the compound **1** skeleton, the alternate $[\text{VO}_4]$ tetrahedron of the $[\text{V}_4\text{O}_{12}]^{4-}$ subunit coordinates to one $[\text{Zn}(\text{eIM})_3]^{2+}$ ion by the terminal O atoms on the same side of the *pseudo*-plane formed by the $[\text{V}_4\text{O}_{12}]^{4-}$.

In the crystal structure of compound **1**, each $[\text{VO}_4]^{3-}$ tetrahedron in the $[\text{V}_4\text{O}_{12}]^{4-}$ units can further coordinate one $\text{Zn}(\text{II})$ ion by the terminal O atom to form an extended 2D folded structure. As shown in Fig. 2a, the $[\text{V}_4\text{O}_{12}]^{4-}$ units bridged with $\text{Zn}(\text{II})$ along the crystallographic *c*-axis can form a 1D chain, in which $[\text{V}_4\text{O}_{12}]$ coupled to two different Zn ions, and the 1D chain further connected with the symmetrical $\text{Zn}(\text{II})$ ions along the crystallographic *c*-axis lead to the formation of a 2D network, in which four $[\text{V}_4\text{O}_{12}]$ units connected with four $\text{Zn}(\text{II})$ ion forming an elliptic eight-member ring. Different from the former study [16], two neighboring V–O–Zn atoms point to the same direction. In the extended 2D folded network, the elliptic eight-member ring linked

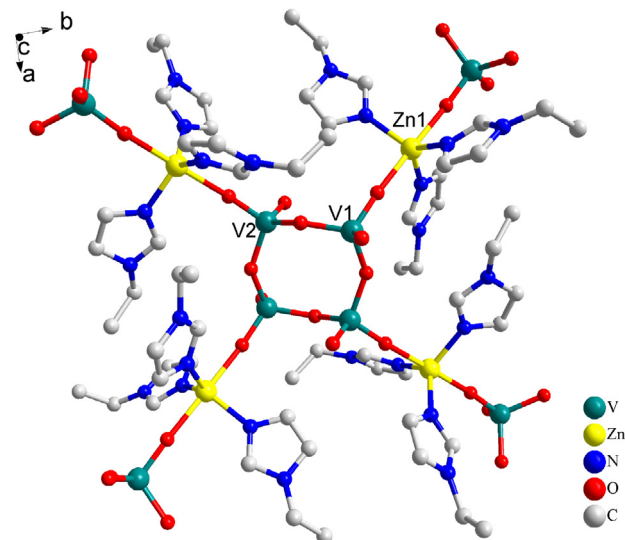


Fig. 1. Ball-and-stick representation of coordination environment of the central atoms V and Zn in compound **1**, hydrogen atoms are not included for clarity.

with four $\text{Zn}(\text{II})$ imidazole modified metal–organic subunits, and the coordinated eIM ligands arrange in the eight-member rings view are different, as shown in Fig. 2b.

3.3. Structure description of compound **5**

When we change the transition metal and retain the rest of the synthetic conditions as used in the synthesis of **4**, compound **5** was isolated when the reaction mixture was cooled to room temperature. According to the SXRD and element analysis, the structural formula of compound **5** is $[\text{Cu}(\text{eIM})_2(\text{H}_2\text{O})]_2\text{V}_4\text{O}_{12}$, which is a 1D inorganic–organic hybrid vanadate and crystallizes in the $\text{P2}_1/\text{n}$ space group. The 1D chain is built from the connection of secondary building units $[\text{V}_4\text{O}_{12}]^{4-}$ and eIM ligands modified

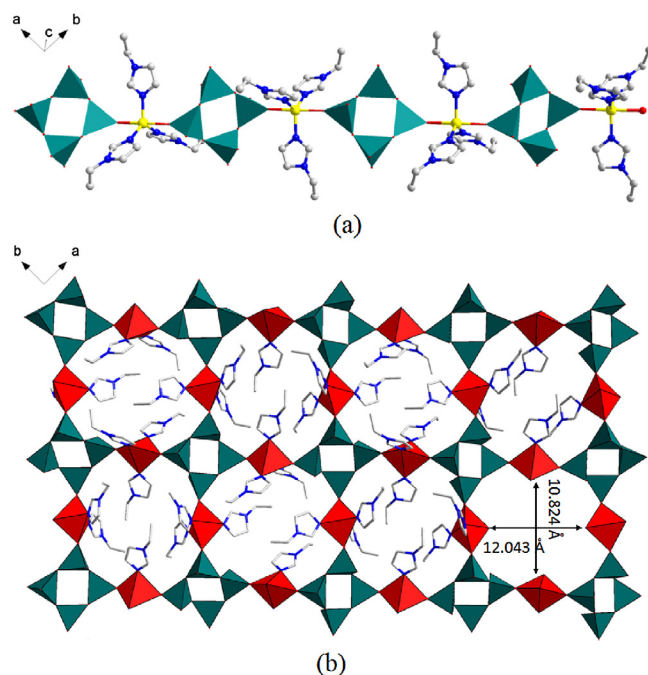


Fig. 2. (a) The 1D chain structure in compound **1**. (b) Polyhedral view of the 2D folded network in $[\text{Zn}(\text{eIM})_3]_2\text{V}_4\text{O}_{12}$. Color code: $[\text{V}_4\text{O}_{12}]$ cluster, green; $[\text{ZnN}_3\text{O}_2]$ hexahedron, red.

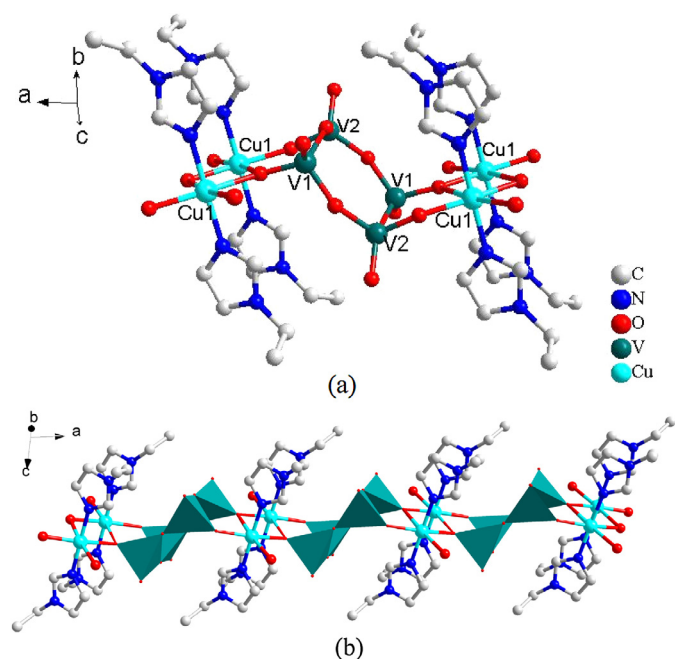


Fig. 3. (a) Ball-and-stick representation of coordination environment of the central atoms V and Cu in compound **5**, hydrogen atoms are not included for clarity. (b) The packing structure representation of the 1D chain in the crystal structure of compound **5**. Color code: $[V_4O_{12}]$ cluster, green.

metal organic subunits $\{Cu(eIM)_2(H_2O)\}$. As shown in Fig. 3a, all central metal V atoms in the structure exhibit distorted tetrahedral coordination geometry and coordinated by four O atoms and each $[VO_4]$ tetrahedron is linked to other tetrahedron through their vertex, forming the secondary building units $[V_4O_{12}]^{4-}$. As shown in Fig. 3b, the Cu ion in the structure coordinates with two N atoms of two eIM ligands, three O atoms from different $[V_4O_{12}]^{4-}$ units and one H_2O molecule. The 1D chain formed by spontaneous resolution upon crystallization which represents a significant example for the inorganic–organic hybrid materials based on vanadates.

3.4. Powder XRD analyses

To further study the purity and repeatability of these crystals, the collected products were crushed to obtain a fine powder suitable for powder XRD analysis. The powder XRD detection allowed us to confirm that the bulk powder was a single phase material. All peaks are perfectly indexed on the basis of the simulation from single crystal analysis. As shown in Fig. S1 (Supporting information), the diffraction peak positions of the experimental PXRD pattern of the products of **1–5** are in good agreement with the simulated patterns from single-crystal X-ray diffraction, indicating the phase purity of samples is satisfactory.

3.5. Thermogravimetric analyses

Thermal analyses of compounds **1–5** were performed under N_2 at a $10^\circ C/min$ rate in the range of $25–800^\circ C$. As shown in Fig. S2 (Supporting information), the TGA analyses indicate that all compounds are stable under $130^\circ C$ and meet the conditions of the catalytic reactions. Besides, the thermogravimetric analysis diagrams of compounds **1**, **3**, **4** and **5** show one main step in the range of $130–550^\circ C$ and $130–450^\circ C$, respectively, and give a total loss of 53.7%, 57.2%, 48.6% and 48.6%. TGA curves of compound **2** display a two-step continuous weight loss. The first weight loss is

5.2% in the temperature range $60–130^\circ C$, assigned to the removal of one crystal water, followed by a loss of 52.0%, corresponding to the release of 1-ethimidazole ligands from $130^\circ C$ to $450^\circ C$. The whole weight loss of 57.2% is consistent with the calculated value of 56.9%.

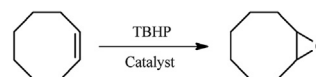
3.6. FT-IR spectra

The IR spectra of compounds **1–5** were performed in the $4000–400\text{ cm}^{-1}$ range. All compounds display similar characteristic vibration patterns mainly resulting from the eIM/pIM/ipIM ligands and vanadate groups. As shown in Fig. S3 (Supporting information), characteristic bands in the range of $1500–1600\text{ cm}^{-1}$ can be attributed to the $C=C$ and $C=N$ stretch modes of the eIM/pIM/ipIM. Peaks associated with $C=C-H$ vibrational modes can be clearly observed at 3101 cm^{-1} for **1**, 3108 cm^{-1} for **2**, and 3101 cm^{-1} for **3**, 3106 cm^{-1} for **4**, 3127 cm^{-1} for **5**, respectively. The characteristic absorption bands of the methyl group appear at $1100–1280$ and $2700–2900\text{ cm}^{-1}$. Besides, coordinated water involved in hydrogen bonding could be positioned by absorption bands around $3400–3560\text{ cm}^{-1}$. Bands below 1000 cm^{-1} are principally assigned to inorganic groups vibrational modes and two types of oxygen atoms: O_t (terminal oxygen atoms), and O_b (bridging oxygen atoms). Specifically, the terminal $V=O_t$ stretching bands appear at 964 cm^{-1} for **1**, 943 cm^{-1} for **2**, 949 cm^{-1} for **3**, 954 cm^{-1} for **4**, and 932 cm^{-1} for **5**. Bands at 789 and 650 cm^{-1} for **1**, 789 and 656 cm^{-1} for **2**, 782 and 664 cm^{-1} for **3**, 793 and 661 cm^{-1} for **4**, 800 , 751 and 647 cm^{-1} for **5** can be assigned to the bridging $M-O-M$ ($M = V, Zn, Co, Cu$) vibrations.

3.7. Catalytic activities of hybrid vanadates

The epoxidation of cyclooctene was selected as a model reaction to evaluate the catalytic activity of compounds **1–5** (Scheme 1). In a typical epoxidation reaction, cyclooctene and TBHP were stirred in a 1:2 ratio in the presence of 1 mol% of catalyst at $70^\circ C$ for 24 h in MeCN. Under aforementioned conditions, the reaction took place smoothly and the epoxide product, formed in good selectivity. As shown in Table 1, compounds **1–5** all can efficiently catalyze the epoxidation of cyclooctene to the corresponding epoxide with the conversion of 93.9%–97.1% and selectivity of 94.7%–100%. Among them, compound **5** showed slightly lower activity than the other compounds under optimized conditions. As a heterogeneous catalyst, compounds **1–4** with a 2D network might provide more active sites exposed to reactants than compound **5** with 1D chain structure [22].

In order to probe the role of each active center of compound **1** in the epoxidation of cyclooctene, we further studied the activity of $Zn(OAc)_2 \cdot 2H_2O$, $CoCl_6 \cdot 6H_2O$, $CuCl_2 \cdot 2H_2O$ and $(n-Bu_4N)_4[V_4O_{12}]$ [29]. As shown in Table 1, the conversion of cyclooctene is quite low when using these simple metal salts as a catalyst, but $(n-Bu_4N)_4[V_4O_{12}]$ led to different a result: the conversion of cyclooctene reached to 67.4%. From the above results, we can conclude that the combination of metal ions (Zn^{2+} , Cu^{2+} , Co^{2+}) and the vanadate anion cluster can produce satisfactory conversion in the catalytic epoxidation of cyclooctene. We surmise that the cooperation between transition metal cations and POV anions in these compounds might synergistically impact the catalytic olefin



Scheme 1. Epoxidation of cyclooctene using hybrid vanadates as catalysts under the preliminary optimization conditions.

Table 1

Comparison of activity and selectivity of different catalysts for cyclooctene to cyclooctane-epoxide^a.

Catalyst	Conv. (%)	Sele. (%)	Reaction system
1	97.1	100	Heterogeneous
2	96.3	95.0	Heterogeneous
3	96.2	95.0	Heterogeneous
4	96.1	95.3	Heterogeneous
5	93.9	94.7	Heterogeneous
Blank	10.1	95.0	
(<i>n</i> -Bu ₄ N) ₄ [V ₄ O ₁₂] ^b	67.4	65.8	Homogeneous
Zn(OAc) ₂ ·2H ₂ O ^c	12.9	89.8	Homogeneous
CoCl ₂ ·6H ₂ O ^c	24.1	93.4	Homogeneous
CuCl ₂ ·2H ₂ O ^c	13.1	88.5	Homogeneous

^a Reaction conditions: Cyclooctene (1 mmol, 1 equiv.), catalyst (0.01 mmol, 1 mol%), TBHP (2 mmol, 2 equiv.), acetonitrile (2 mL), 70 °C, 24 h.

^b V content equivalent to **1**.

^c Zn content equivalent to **1**, Co content equivalent to **4**, Cu content equivalent to **5**.

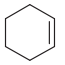
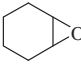
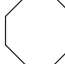
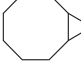
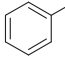
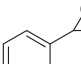
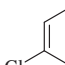
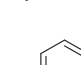
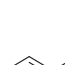
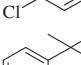
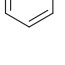
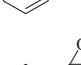
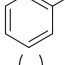
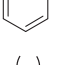
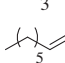
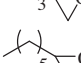
process, which led to the improvement of the resultant catalytic performance [20,22]. More importantly, the participation of the transition metal ions also endowed the catalysts with heterogeneous behavior, which may have potential applications in the industry.

Recyclability is one of the greatest advantages of heterogeneous catalysts and can also provide useful information about the catalyst stability along the catalytic cycle. For the excellent performance, compound **1** is selected to examine the long-term stability in a heterogeneous system. After the completion of the reaction, the catalyst can be easily separated from the reaction mixture by filtration and further reused directly in the subsequent epoxidation reactions. The catalyst was recycled for at least 5 runs and still maintained its conversion (92.0%–97.1%) and selectivity (93.1%–100%) (Table S2 in Supporting information). The PXRD and IR spectra (Figs. S4 and S5 in Supporting information) of **1** after the catalytic reactions indicate that no significant changes were shown by comparing with those of the freshly obtained catalysts. To check the heterogeneity of **1**, a hot filtration experiment (separation of catalyst at the reaction temperature) was carried out. When **1** was filtrated off after 3 h (conv. 40.5%, prod.30.3% of epoxide) and the supernatant was then allowed to react under the same condition, after 21 h, the conversion is found to be 46.1%, which was obviously lower than that in the presence of **1** (97.1%) (Fig. S6 in Supporting information). The results further indicate that **1** has good stability during the oxidation reaction. The heterogeneity of the reaction was also probed by a leaching test with **1** after the third reaction cycle. Atomic absorption analysis of the liquid phase after separation of the catalyst showed that there was no leaching of the V ions from the catalyst to the reaction mixture (Fig. S7 in Supporting information).

The generality of **1** for epoxidation was examined using various olefins with different electronic and steric characters under optimized conditions. As shown in Table 2, the compound showed potential and selectivity as catalyst in the epoxidation of alkenes at 70 °C using TBHP as an oxidant. Notably, compared with styrene, a slight decrease of the catalytic is observed for the electron-deficient 4-Cl-styrene. For the epoxidation of styrene and 4-Cl-styrene, the byproducts are benzaldehyde and 4-chlorobenzaldehyde, and for the epoxidation of α -methylstyrene the byproduct is methylacetophenone. In the epoxidation of *trans*-stilbene, the conversion and selectivity is up to 100%. The applicability of the catalytic activity was further extended to the epoxidation of various cyclic olefins. All cyclic olefins show high selectivity toward the corresponding

Table 2

Results of epoxidation of various olefin catalyzed by **1** using TBHP as oxidant^a.

Entry	Olefin	Products	Conv. (%)	Sele. (%)
1			89.0	89.5
2			97.1	100
3			98.7	65.7
4			90.1	65.6
5			99.8	65.2
6			100	100
7			53.5	96.1
8			57.6	93.2

^a Reaction conditions: Olefin (1 mmol, 1 Eq.), catalyst (0.01 mmol, 1 mol%), TBHP (2 mmol, 2 Eq.), acetonitrile (2 mL), 70 °C, 24 h.

epoxides (Table 2, entries 1,2). In addition, we performed the catalytic activity for some terminal alkenes (R-C=CH₂, R = aliphatic), the conversion of 1-hexene (entry 7, 53.5%) and 1-octene (entry 8, 57.6%) was drastic decreased. Therefore, we can conclude that the heterogeneous catalysts compound **1** is suitable for the epoxidation of cyclic olefins and R-C=CH₂ (R = aromatic).

4. Conclusion

To summarize, we successfully prepared five inorganic–organic hybrid vanadates in the hydrothermal environment under similar conditions. Among them, compounds **1–4** are 2D folded network architectures while **5** has a 1D ladder chain structure. Importantly, all hybrid vanadates show high activity and productivity in the epoxidation of olefins. Noticeably, compound **1** can convert olefins to the corresponding epoxides efficiently and can be reused by filtration with little loss of its activity. To our knowledge, this is the first time that inorganic–organic hybrid vanadates are used as catalysts in the epoxidation of olefins. The rational controllable synthesis of other hybrid vanadates and the use of them in other catalytic reactions are in progress.

Acknowledgments

This work was financially supported by the National Natural Science Foundation of China (Nos. 21173021, 21231002, 21271025 and 21276026), 973 Program (No. 2014CB932103), the 111 Project (No. B07012) and Beijing Higher Education Youth Elite Teacher Project (No. 1209).

Appendix A. Supplementary data

Supplementary data associated with this article can be found, in the online version, at <http://dx.doi.org/10.1016/j.cclet.2016.01.007>.

References

- [1] B.M. Trost, The atom economy—a search for synthetic efficiency, *Science* 254 (1991) 1471–1477.
- [2] M. Tonigold, Y. Lu, D. Volkmer, et al., Heterogeneous catalytic oxidation by MFU-1: a cobalt(II)-containing metal–organic framework, *Angew. Chem. Int. Ed.* 48 (2009) 7546–7550.
- [3] J. Rich, E. Manrique, I. Romero, et al., Catalytic activity of chloro and triflate manganese(II) complexes in epoxidation reactions: reusable catalytic systems for alkene epoxidation, *Eur. J. Inorg. Chem.* 2014 (2014) 2663–2670.
- [4] S. Caron, J.A. Ragan, D.H.B. Ripin, et al., Large-scale oxidations in the pharmaceutical industry, *Chem. Rev.* 106 (2006) 2943–2989.
- [5] B.S. Lane, K. Burgess, Metal-catalyzed epoxidations of alkenes with hydrogen peroxide, *Chem. Rev.* 103 (2003) 2457–2474.
- [6] M. Herbert, E. Alvarez, A. Galindo, et al., Olefin epoxidation by hydrogen peroxide catalysed by molybdenum complexes in ionic liquids and structural characterization of the proposed intermediate dioxoperoxomolybdenum species, *Chem. Commun.* 46 (2010) 5933–5935.
- [7] C.J. Thibodeaux, W.C. Chang, H.W. Liu, Enzymatic chemistry of cyclopropane, epoxide, and aziridine biosynthesis, *Chem. Rev.* 112 (2012) 1681–1709.
- [8] K. Girijesh, K. Gulshan, G. Rajeev, Manganese- and cobalt-based coordination networks as promising heterogeneous catalysts for olefin epoxidation reactions, *Inorg. Chem.* 54 (2015) 2603–2615.
- [9] S.T. Oyama, in: S.T. Oyama (Ed.), *Mechanisms in Homogeneous and Heterogeneous Epoxidation Catalysis*, Elsevier, Amsterdam, 2008, pp. 1–99.
- [10] J. Hagen, *Industrial Catalysis: A Practical Approach*, Wiley-VCH, Weinheim, 1999.
- [11] J.M. Breen, W. Schmitt, Hybrid organic–inorganic polyoxometalates: functionalization of V^{IV}/V^{V} nanosized clusters to produce molecular capsules, *Angew. Chem. Int. Ed.* 120 (2008) 7010–7014.
- [12] E. Antonova, C. Näther, P. Köerler, W. Bensch, Die organische funktionalisierung von polyoxovanadaten: Sb–N-Bindungen und Ladungskontrolle, *Angew. Chem. Int. Ed.* 123 (2011) 790–793.
- [13] P. Köerler, B. Tsukerblat, A. Müller, Structure-related frustrated magnetism of nanosized polyoxometalates: aesthetics and properties in harmony, *Dalton Trans.* 39 (2010) 21–36.
- [14] B.K. Chen, Y.N. Chi, C.W. Hu, et al., Three new imidazole-functionalized hexanuclear oxidovanadium clusters with exceptional catalytic oxidation properties for alcohols, *Chem. Eur. J.* 19 (2013) 4408–4413.
- [15] E.S. Larrea, J.L. Mesa, M.I. Arriortua, et al., $M(C_6H_{16}N_3)_2(VO_3)_4$ as heterogeneous catalysts. Study of three new hybrid vanadates of cobalt(II), nickel(II) and copper(II) with 1-(2-aminoethyl)piperazonium, *Dalton Trans.* 40 (2011) 12690–12698.
- [16] R.F. de Luis, M.K. Urtiaga, M.I. Arriortua, et al., Thermal response, catalytic activity, and color change of the first hybrid vanadate containing bpe guest molecules, *Inorg. Chem.* 52 (2013) 2615–2626.
- [17] H. Lin, P.A. Maggard, Synthesis and structures of a new series of silver–vanadate hybrid solids and their optical and photocatalytic properties, *Inorg. Chem.* 47 (2008) 8044–8052.
- [18] Y. Hu, F. Luo, F. Dong, Design synthesis and photocatalytic activity of a novel lilac-like silver–vanadate hybrid solid based on dicyclic rings of $[V_4O_{12}]^{4-}$ with $\{Ag_7\}^{7+}$ cluster, *Chem. Commun.* 47 (2011) 761–763.
- [19] L. Luo, P.A. Maggard, Effect of ligand coordination on the structures and visible-light photocatalytic activity of manganese vanadate hybrids, *Cryst. Growth Des.* 13 (2013) 5282–5288.
- [20] J.K. Li, X.Q. Huang, Y.N. Chi, C.W. Hu, Four alkoxohexavanadate-based Pd–Polyoxovanadates as robust heterogeneous catalysts for oxidation of benzyl–alkanes, *Inorg. Chem.* 54 (2015) 1454–1461.
- [21] S.J. Wu, Z.G. Lin, C.W. Hu, et al., Synthesis, structure and characterization of three different dimension inorganic–organic hybrid vanadates: $[Co_2(mIM)_5(-H_2O)_2]V_4O_{12}$, $[Ni_2(mIM)_7(-H_2O)]V_4O_{12} \cdot H_2O$ and $[Cd(eIM)_2(H_2O)]V_2O_6$, *CrystEngComm* 17 (2015) 1625–1630.
- [22] J.K. Li, X.Q. Huang, C.W. Hu, et al., Controllable synthesis, characterization, and catalytic properties of three inorganic–organic hybrid copper vanadates in the highly selective oxidation of sulfides and alcohols, *Cryst. Growth Des.* 15 (2015) 1907–1914.
- [23] G. Kummar, G. Kummar, R. Gupta, Manganese- and cobalt-based coordination networks as promising heterogeneous catalysts for olefin epoxidation reactions, *Inorg. Chem.* 54 (2015) 2603–2615.
- [24] L. Tabrizi, H. Chiniforoshan, P. Mardle, A cobalt(II) complex with anionic and neutral N-donor ligands: synthesis, crystal structure, and application as a heterogeneous catalyst for olefin epoxidation with *tert*-BuOOH, *J. Coord. Chem.* 68 (2015) 980–992.
- [25] J.K. Gao, L.L. Bai, Q.H. Zhang, et al., $Co_6(\mu_3-OH)_6$ cluster based coordination polymer as an effective heterogeneous catalyst for aerobic epoxidation of alkenes, *Dalton Trans.* 43 (2014) 2559–2565.
- [26] M. Sankaralingam, M. Palaniandavar, Tuning the olefin epoxidation by manganese(III) complexes of bisphenolate ligands: effect of Lewis basicity of ligands on reactivity, *Dalton Trans.* 43 (2014) 538–550.
- [27] G.M. Sheldrick, *SHELXTL NT/ v. 6.14*, Bruker Analytical X-ray Systems, Madison, Wisconsin, 2000.
- [28] G.M. Sheldrick, *SHELXS-97: Program for Crystal Structure Solution*, Göttingen University, Göttingen, Germany, 1997.
- [29] J. Forster, B. Rösner, M.M. Khusniyarov, C. Streb, Tuning the light absorption of a molecular vanadium oxide system for enhanced photooxidation performance, *Chem. Commun.* 47 (2011) 3114–3116.